REPORT DOCUMENTATION PAGE

Form Approved OMB No. 0704-0188

1. REPORT DATE *(DD-MM-YYYY)*	2. REPORT TYPE	3. DATES COVERED *(From – To)*
23-09-2005	Final Report	1 July 2004 - 01-Jul-05

4. TITLE AND SUBTITLE

Modeling of Power Combining in Microstrips with Arrays of Active Devices - Josephson Junctions and Gunn Diodes - for THz Applications

5a. CONTRACT NUMBER
FA8655-04-1-3027

5b. GRANT NUMBER

5c. PROGRAM ELEMENT NUMBER

6. AUTHOR(S)

Dr. Vladimir Yurchenko

5d. PROJECT NUMBER

5d. TASK NUMBER

5e. WORK UNIT NUMBER

7. PERFORMING ORGANIZATION NAME(S) AND ADDRESS(ES)
National University of Ireland
Maynooth
Ireland

8. PERFORMING ORGANIZATION REPORT NUMBER
N/A

9. SPONSORING/MONITORING AGENCY NAME(S) AND ADDRESS(ES)

EOARD
PSC 821 BOX 14
FPO 09421-0014

10. SPONSOR/MONITOR'S ACRONYM(S)

11. SPONSOR/MONITOR'S REPORT NUMBER(S)
Grant 04-3027

12. DISTRIBUTION/AVAILABILITY STATEMENT

Approved for public release; distribution is unlimited.

13. SUPPLEMENTARY NOTES

14. ABSTRACT

This report results from a contract tasking National University of Ireland as follows: The Grantee will investigate methods to increase power output of THz arrays. Simulations will be used to build models of various array structures.

15. SUBJECT TERMS
EOARD, Electronic Devices

16. SECURITY CLASSIFICATION OF:			17. LIMITATION OF ABSTRACT	18. NUMBER OF PAGES	19a. NAME OF RESPONSIBLE PERSON
a. REPORT	b. ABSTRACT	c. THIS PAGE			MICHAEL KJ MILLIGAN, Lt Col, USAF
UNCLAS	UNCLAS	UNCLAS	UL	26	19b. TELEPHONE NUMBER *(Include area code)* +44 (0)20 7514 4955

Modeling of Power Combining in Microstrips with Active Devices for THz Applications

Vladimir Yurchenko
Experimental Physics Dept., NUI Maynooth, Ireland

August 29, 2005

Abstract

Self-consistent time-domain simulations of active systems with Gunn diodes connected by sections of microstrip transmission lines (TL) are carried out. Nonlinear power combining of Gunn diodes mounted in various ways in the TL circuits has been studied. Complex dynamics of the electromagnetic field radiated into an open end of the TL are observed including single-frequency oscillations, multi-frequency generation, and the dynamical chaos which could be accompanied by multi-frequency generation. Trains of high-frequency pulses are shown to emerge in such systems when active devices are separated from compact resonant circuits by extended sections of the TL providing a time-delayed feedback.

1 Introduction

We perform computer simulations of nonlinear power combining in distributed microstrip transmission line systems with active THz devices specified by negative differential resistance (NDR) of current-voltage characteristics such as of Gunn diodes and similar structures.

There are two **major goals** of this research which concern both the theoretical and practical aspects of the problem:

- Developing mathematical models, numerical techniques and computer codes for the efficient self-consistent time-domain simulation of high-frequency excitation in distributed systems with a strong time-delayed coupling between active devices connected by sections of transmission lines (TL);
- Studying available options of microstrip implementation of nonlinear power combining (superlinear in the number of devices) and non-conventional spectral effects (ultra-wideband chaotic oscillations etc) for possible practical applications in various high-frequency electronic systems (ultra-short pulse generation, noise radars, etc).

Microwave power combining has been studied for a long time in a variety of systems. Initially, there were lumped circuits being considered. Later on, waveguide circuit solutions [1], [2] and quasi-optical array systems [3], [4] have been proposed.

Despite these efforts and numerous achievements [4], [5], efficient power combining remains a challenging problem in all aspects including the theoretical analysis, numerical simulations, engineering design, and practical implementation. There are important physical reasons for this, such as intrinsically complicated nonlinear nature of the phenomena, distributed character of the systems whose size is large compared to the wavelength (especially, when considering open radiating systems), broadband and multi-frequency dynamics of oscillations, etc.

Nowadays, the major goal in this area is the efficient power combining in the THz domain where the output power of individual devices is intrinsically limited by the physical processes

involved (the main relaxation channels in both the devices and the environment occur precisely in this domain). In the meantime, the main difficulties of power combining (nonlinearity, distributed systems, complex broadband dynamics) are the most significant for the THz systems since the size of a multi-device structure typically exceeds a sub-mm wavelength and the inter-device coupling is particularly strong in such cases.

In terms of the design and simulation of active THz systems, there is a lack of appropriate analysis methods and computation techniques. This restricts both the design of real structures and the understanding of processes involved. Conventional microwave design and analysis tools [6], [7] (e.g., the impedance analysis) are insufficient, being only valid in a small-signal approximation for narrow-band systems. On the other hand, advanced numerical methods (e.g., [8]) require huge computational resources and become inefficient.

The active character of the devices specified by intrinsic instability and nonlinearity makes common simulation tools (e.g., Flomerics Micro-Strips etc) inadequate for the rigorous modeling of such systems. Other software, such as SPICE, cannot cope with distributed systems where the wave propagation between the devices is an essential part of the system operation. A promising approach is the hybrid numerical methods [9] which combine both the frequency-domain and the time-domain computations, though they also suffer from various limitations (narrow-band approximation etc).

For these reasons, the design of active structures is usually split in two separate stages dealing with either linear or nonlinear parts of the system. In this approach, the attention is focused on passive components whose design is carried out in much detail, though in a conventional manner. As a price for this simplification, some assumptions are supposed to be met such as the operation of the system in the narrow band or in a given set of a few narrow bands, etc.

In this work, we choose an alternative approach and focus our attention on the nonlinear part of the problem, while the linear part is chosen to be relatively simple.

In this approach, the aim is the accurate *self-consistent modeling* of nonlinear effects through rigorous solutions of governing equations and, specifically, accurate time-domain simulations of nonlinear oscillations and *non-conventional dynamics* (chaos, pulses) emerging in various conditions. As a practical issue, nonlinear power combining is investigated in a rigorous manner.

By reducing the linear part of the problem to the simplest form, we arrive at the set of discrete devices connected by sections of one-dimensional transmission lines, e.g., microstrips. Microstrips excited by solid-state devices are rather practical solutions for various applications. A study of one-dimensional models provides also a benchmark for testing computational methods ranging from analytic approximations to advanced numerical tools.

In quasi-optical applications, parallel coupling of active devices in a single array is used for increasing the power output from the system [4] (in microwaves, similar ideas were implemented in the waveguides [1]). A one-dimensional analogue of this system is the **parallel connection** of transmission line circuits, with the microwave power being radiated into an open infinite section of the line (the latter models the radiation of the electromagnetic waves from the antennas into the free space in three-dimensional open systems).

As an alternative system, a **series connection** of active devices in a long transmission line (a ladder-type oscillator) represents a simple model of an open active structure with distributed elements that could be used for the efficient spectrum modification of THz radiation. Recent simulations of a chain of Gunn diodes [10], revealed an interesting dynamics of the electromagnetic field in this system, though more detailed analysis of this structure is required.

The interest in the systems of this kind is justified by their potential applications as the sources of chaotic signals for the emerging field of the noise radar technology [11]. This technology provides a number of benefits such as an ultra-wideband spectrum of radiation, simultaneous detection of the position and the velocity of the target, operation below the noise level of the environment, and other advantages. For these reasons, THz applications and, especially, MMIC implementations of these systems are of particular interest.

2 Time-delay TL circuits of active devices

Time-delay TL circuits with active devices could be of different kind, for example, as those shown schematically in Fig. 1. Extended sections of the transmission lines (microstrips) of length d_n provide the time-delayed coupling between the lumped circuits of active devices ($n = 1 \ldots N$) which could also be of different kind (Figs. 2, 3) and could be connected either in parallel (in a radial connection with an "antenna node" $n = 0$, Fig. 1, a) or in series (in a ladder-type oscillator, Fig. 1, b). In both cases, the structure is connected to an infinite section of the TL as shown in Fig. 1, a and b, at the left side so that the entire system is open and the waves generated by the devices are radiated towards the infinity $x = -\infty$, thus, simulating the radiation of the electromagnetic waves by the antennas in three-dimensional space.

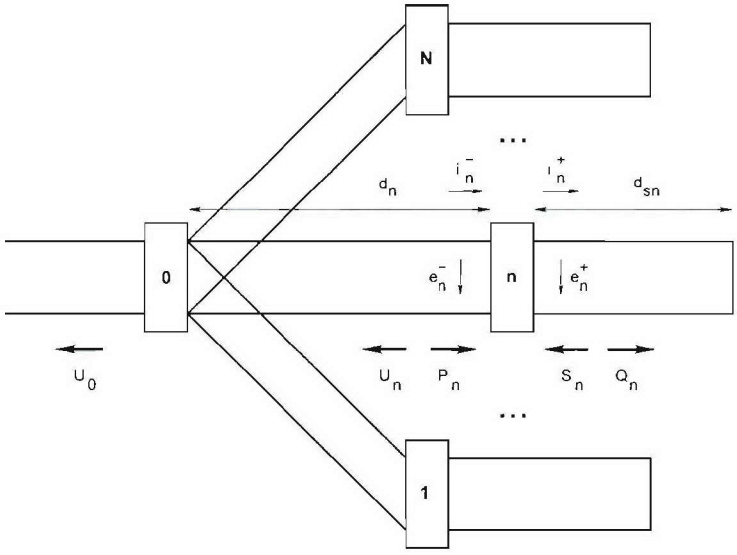

(a)

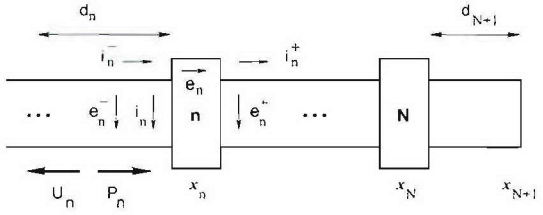

(b)

Figure 1: Transmission line systems with parallel and series connection of active circuits

The active circuits are considered of a simple though generic form. They include the nonlinear active device G_n (the Gunn diode), the resistance R_n, the bias voltage V_{B_n}, the inductance L_n and the capacitance C_n connected in various manner in the circuit and, via the circuit ports, in the microstrip line (see Figs. 2 and 3, a and b).

The antenna nodes $n = 0$ in the parallel connection of circuits are also assumed of different kinds, Fig. 4, a and b. The capacitance C_A in the case "a" prevents the direct current from flowing into the infinite section of the TL (this allows a more realistic simulation of three-dimensional radiating systems), while the resistance R_T (the conductance $S_T = 1/R_T$) is used for the additional dumping of current ($S_T = 0$ is assumed in most cases). The node circuit "b" is essentially a lumped resonant LC circuit being precisely of the same kind as the equivalent LC circuit in the waveguide power combining structures considered in Ref [1].

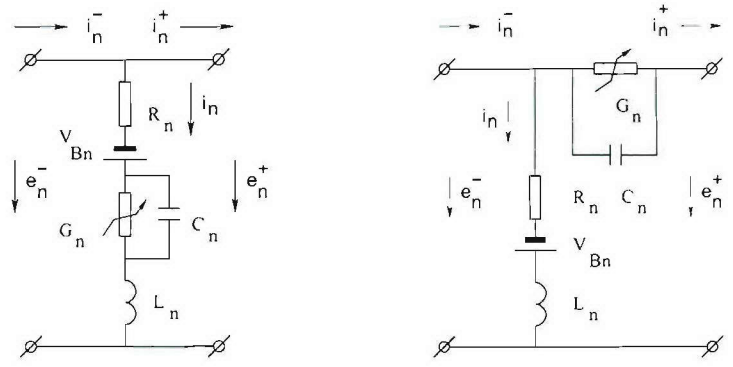

Figure 2: Active circuits considered in the case of series connection

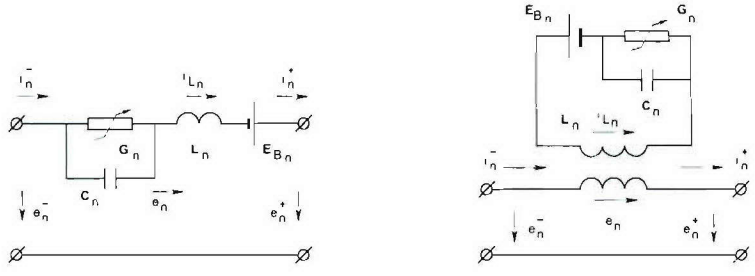

Figure 3: Active circuits considered in the case of parallel connection

Formulation of the problem is provided by the set of equations consisting of

(i) the wave equations for the current $i_n(\tau, x)$ and voltage $e_n(\tau, x)$ in each section n of the microstrip transmission line $(x_{n-1} < x < x_n)$,

(ii) the circuit equations for each circuit n written in terms of the current $i_n(\tau)$ and voltage $e_n(\tau)$ defined appropriately for each circuit as shown in Figs. 2 – 4, and

(iii) the boundary conditions for the wave equations at the points of microstrip connections to the circuits $(x_n^{\pm} = x_n \pm 0)$ which establish the link between the microstrip currents and voltages at the points $x_n^{\pm}$ $(i_n^{\pm}(\tau) = i_n(\tau, x_n^{\pm}),\ e_n^{\pm}(\tau) = e_n(\tau, x_n^{\pm}))$ and the circuit currents $i_n(\tau)$ and voltages $e_n(\tau)$ as shown in Figs. 1 – 4.

The set of equations is completed by the radiation condition at $x = -\infty$ (no incoming waves from the open end of the transmission line) and the short-circuit condition providing the wave reflection at the ends of the stubs (e.g., $e_{N+1}^{-}(\tau) = 0$ at $x = x_{N+1}^{-}$ in Fig. 1, b).

Notice that all the equations in this work are written in terms of dimensionless normalized variables such as the relative coordinate $x = X/a$, time $\tau = ct/a$, voltage $e_n = V_n/V_0$ and current $i_n = Z_0 I_n/V_0$ where a is the spatial scale used for normalization, c is the speed of wave in the transmission line, Z_0 is the intrinsic impedance of the line, V_0 is the normalization voltage. In a similar way, we introduce other dimensionless parameters such as $r_n = R_n/Z_0$, $\tau_{C_n} = cZ_0C_n/a$, $\tau_{L_n} = cL_n/(Z_0a)$, etc.

The Gunn diodes are simulated in terms of the given current-voltage characteristics with negative differential resistance (NDR) as shown in Fig. 5. This approximation assumes the limited space-charge accumulation (LSA) mode of operation of Gunn diodes. This allows a rather broadband functioning of the devices, with the maximum-to-minimum frequency ratio exceeding

a decade. The approximation means an instant response of the diodes to the external field neglecting the modeling of strong-field domains in the diode structures. Instead, characteristic times of intrinsic processes specific for the diodes are represented by the equivalent capacitance C_n and the inductance L_n of the devices and their connections to the circuits.

(a) (b)

Figure 4: Circuits considered as an antenna node ($n = 0$) or a resonant chain ($n = N_{LC}$)

The current-voltage characteristic of the diodes is given by the approximation [12] typical for GaAs and GaN structures:

$$G_n = G_n(e) = G_{0_n} f(e) = G_{0_n}[(e + 0.2e^4)/(1 + 0.2e^4) + 0.05e] \tag{1}$$

where $G_{0_n} = Z_0 I_{0_n}/V_0$ is the dimensionless diode current parameter, I_{0_n} and V_0 are the characteristic absolute current and voltage specifying the diodes (e.g., for the L-band GaN THz Gunn diodes described in [13], we have $I_{0_n} \approx 8A$, $V_0 \approx 30V$), and, finally, $e = |e_{G_n}|$ is the dimensionless voltage applied to the diode (Fig. 5).

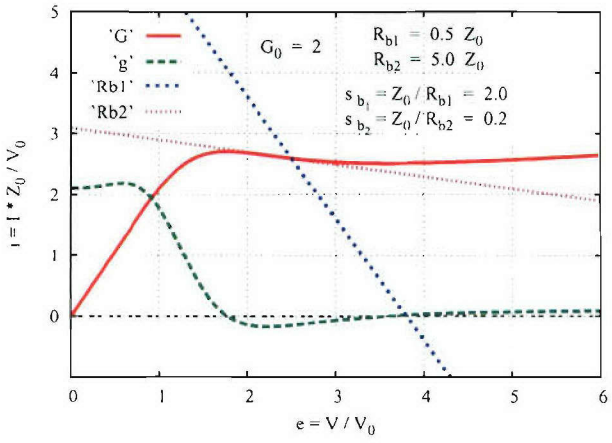

Figure 5: The Gunn diode current-voltage characteristic $i = G(e)$, the differential conductance $g = di/de$, and the load lines at the bias resistance r_B

The wave equations for the TL currents and voltages take on the form

$$\frac{\partial e_n}{\partial x} = -\frac{\partial i_n}{\partial \tau}, \qquad \frac{\partial e_n}{\partial \tau} = -\frac{\partial i_n}{\partial x}. \tag{2}$$

The circuit equations are defined by the composition of particular circuits as considered in the following sections. Finally, the boundary conditions are specified by the type of the circuit and the way of its connection to the microstrip line.

The electromagnetic self-excitation appears in the system when the Gunn diodes are biased to the NDR region. The oscillations develop in response to a small fluctuation of the bias voltage,

once the voltage is in this region, or as a result of switching the bias from the stable to this unstable domain.

The bias voltage $e_B(\tau)$ is specified by the function

$$e_B(\tau) = e_{B_0} + \delta e_B f_B(\tau/\tau_S) - \delta e_B f_B((\tau - \tau_F)/\tau_S) \tag{3}$$

where e_{B_0} is the steady-state voltage in the "off" position below the threshold $e_{B_{th}}$ when no self-oscillations are excited (the oscillations appear if $e_B > e_{B_{th}}$), $e_{B_1} = e_{B_0} + \delta e_B$ is the steady-state voltage in the "on" position when self-oscillations are being developed ($e_{B_1} > e_{B_{th}}$), $f_B(\tau/\tau_S)$ is the bias switch function which describes the switching on and off process beginning at the moment $\tau = 0$ and $\tau = \tau_F$, respectively, and developing during the characteristic time τ_S ($0 \le f_B \le 1$, $f_B = 0$ at $\tau \le 0$, $f_B = 1$ at $\tau \ge \tau_S$).

As a switch function, we choose $f_B = (\tanh(u) + 1)/2$ with the substitution $u = s/(1 - s^2)$, $s = 2\tau/\tau_S - 1$, defined in the interval $|s| < 1$ where $0 \le f_B \le 1$ ($f_B = 0$ at $s = -1$, $f_B = 1$ at $s = 1$), while outside of this interval we assign $f_B = 0$ at $s < -1$ ($\tau < 0$) and $f_B = 1$ at $s > 1$ ($\tau > \tau_S$).

This definition of the switch function f_B allows us to confine the duration of switching on and off within the finite time interval $0 \le \tau \le \tau_S$, with both $df_B/d\tau$ and $d^2 f_B/d\tau^2$ being zero at $\tau \le 0$ and $\tau \ge \tau_S$. Notice, the condition $df_B/d\tau = d^2 f_B/d\tau^2 = 0$ at $\tau \le 0$ is necessary for the consistency of time-delay equations at $\tau \le 0$ with the trivial initial conditions on the unknown functions at the time-delayed intervals while assuming no time variations before the switching on begins.

Despite apparent simplicity of circuits considered, self-consistent time-domain modeling of these distributed systems is a complicated problem. We approach this problem by utilizing a general solution of one-dimensional wave equation following the method of Ref [14] that allows one to reduce the problem of the field evolution in a one-dimensional cavity to the algebraic equation with time-delay. In distinction from Ref [14], in this work we deal with more complicated systems and arrive at a set of differential-difference equations rather than the algebraic-difference one. Also, once considering open radiating systems, we study the radiation emitted by the system towards infinity.

3 Parallel connection of microstrip circuits

In this section, we consider the parallel connection of microstrip lines (Fig. 1, a) with active circuits of Fig. 3, a, when the "antenna circuit" ($n = 0$) is of the kind of Fig. 4, a.

Of the total number of N microstrip lines, we assume to have $N_D = N - 2$ lines with Gunn diodes ($n = 1 \ldots N_D$), one line with a lumped resonant LC circuit of Fig. 4, b ($n = N_{LC} = N-1$), and another line ($n = N$) with the bias circuit similar to Fig. 3, a, where the Gunn diode is replaced by the bias resistor R_B (thus, $N_D \ge 1$, $N \ge 3$).

Typically, we assume the resonant line $n = N_{LC}$ to be of zero length ($d_{N_{LC}} \approx 0$). In this case the central "antenna node" $n = 0$ has intrinsic resonant properties due to the lumped LC circuit $n = N_{LC}$ that makes the system similar to the waveguide structure considered by Kurokawa [1]. Also, we assume $R_0 = \infty$ ($s_0 = Z_0/R_0 = 0$) and suppose $e_{B_n} = 0$ for all active circuits so that the bias is applied to the devices through the common bias line $n = N$ of nonzero length d_N ($e_{B_N} = e_B(\tau) \ne 0$) .

3.1 Formulations for the parallel circuits

To derive the equations for the parallel connection of microstrip circuits, we use the general solutions to the wave equations in the microstrip lines of length d_n and in the stubs of length d_{S_n} in the form of superpositions of waves propagating in opposite directions, e.g., $\Psi_n(\tau - x)$

and $U_n(\tau+x)$, so that the current i_n and voltage e_n in the line section n are presented as follows:

$$i_n = \Psi_n(\tau - x) + U_n(\tau + x), \qquad e_n = \Psi_n(\tau - x) - U_n(\tau + x). \tag{4}$$

By introducing the node coordinates $x_n = d_n$, $x_{S_n} = d_n + d_{S_n}$ ($x_0 = 0$) and the relative time variables for different sections of lines defined as

$$\vartheta_n = \tau + d_n = \tau + x_n, \qquad \vartheta_{S_n} = \vartheta_n + d_{S_n} = \tau + x_{S_n}, \tag{5}$$

we obtain

$$U_n(\tau + x_n) = U_n(\vartheta_n), \qquad \Psi_n(\tau - x_n) = \Psi_n(\vartheta_n - 2x_n) \tag{6}$$

and

$$U_{S_n}(\tau + x_{S_n}) = U_{S_n}(\vartheta_{S_n}), \qquad \Psi_{S_n}(\tau - x_{S_n}) = \Psi_{S_n}(\vartheta_{S_n} - 2x_{S_n}). \tag{7}$$

Then, using new variables

$$P_n(\vartheta_n) = \Psi_n(\vartheta_n - x_n), \quad Q_n(\vartheta_{S_n}) = U_{S_n}(\vartheta_{S_n}), \quad S_n(\vartheta_{S_n}) = \Psi_{S_n}(\vartheta_{S_n} - x_{S_n}), \tag{8}$$

we can express the microstrip currents $i_n^{\pm}$ and voltages $e_n^{\pm}$ at the points $x_n^{\pm}$ of microstrip connections to circuits, $i_n^{\pm}(\tau) = i_n(\tau, x_n^{\pm})$ and $e_n^{\pm}(\tau) = e_n(\tau, x_n^{\pm})$, via the waveforms U_n, P_n, S_n, Q_n representing the relevant waves in the lines and stubs (see Fig. 1, a).

Written for the active, resonant, and bias circuits (with account of the stub boundary condition $e(\tau) = 0$ at $x = x_{S_n}$ that allows to exclude Q_n), the microstrip currents and voltages at the circuit connection points are obtained as follows ($n = 1 \ldots N$):

$$i_n^+(\tau) = S_n(\vartheta_n - 2d_{S_n}) + S_n(\vartheta_n) \tag{9}$$

$$e_n^+(\tau) = -S_n(\vartheta_n - 2d_{S_n}) + S_n(\vartheta_n) \tag{10}$$

$$i_n^-(\tau) = U_n(\vartheta_n) + P_n(\vartheta_n - d_n) \tag{11}$$

$$e_n^-(\tau) = -U_n(\vartheta_n) + P_n(\vartheta_n - d_n). \tag{12}$$

Similarly, the currents and voltages at the antenna node ($n = 0$) are found in the form

$$i_{A_n}^+(\tau) = U_n(\vartheta_n - d_n) + P_n(\vartheta_n) \tag{13}$$

$$e_{A_n}^+(\tau) = -U_n(\vartheta_n - d_n) + P_n(\vartheta_n) \tag{14}$$

$$i_A^-(\tau) = U_A(\tau) \tag{15}$$

$$e_A^-(\tau) = -U_A(\tau) \tag{16}$$

where $U_A(\tau) = U_A(\tau + x_0^-)$ is the wave radiated from the system into an infinite section of microstrip line, when evaluated at the antenna node $x = x_0^-$. In this presentation, the initial conditions are supposed to be of the form $i_A^- = 0$, $e_A^- = 0$ ($U_A = 0$) when $\tau \le 0$, i.e., there is no bias and no excitation at $\tau \le 0$. The radiation condition has also been accounted in this form (there is no incoming wave $P_A(\tau - x_0^-)$ incident on the structure).

Now, we formulate the circuit equations in terms of the circuit currents i_n and voltages e_n defined specifically for each circuit n and relate them with the microstrip currents $i_n^{\pm}$ and voltages $e_n^{\pm}$ at the connection points $x = x_n^{\pm}$.

Using the definitions of currents and voltages as shown for the circuits of Fig. 3, a, the connection equations (the boundary conditions at the nodes x_n) are obtained as follows

$$i_n = i_n^- = i_n^+, \qquad e_n = e_n^- - e_n^+ \tag{17}$$

where the circuit currents and voltages are

$$i_n = i_{L_n} = i_{G_n} + i_{C_n}, \qquad e_n = e_{C_n} + e_{L_n} - e_{B_n}. \tag{18}$$

Here, $i_{G_n} = G_n(e_{G_n})$ is the Gunn diode current at the diode (capacitance) voltage $e_{G_n} = e_{C_n}$, $i_{C_n} = \tau_{C_n} de_{C_n}/d\tau$ is the capacitance current, $e_{L_n} = \tau_{L_n} di_{L_n}/d\tau$ is the inductance voltage, and $e_{B_n} = e_{B_n}(\tau)$ is the given bias voltage.

Eqs. (17) – (18) are valid for all active, resonant and bias circuits as shown in Fig. 3, a, where the relevant parameters should be substituted in each particular case: for the bias circuit ($n = N$) we use $i_{G_N} = s_N e_{G_N}$ as the bias resistance current instead of $G_n(e_{G_n})$ above ($s_N = Z_0/R_N$ is the dimensionless bias conductance), while the LC circuit of Fig. 4, b, with open right contacts ($n = N_{LC}$) is reduced to Fig. 3, a, with a short-circuited stub of zero length, $d_{S_n} = 0$.

In a similar way, we obtain the antenna node connection and circuit equations ($n = 0$). For the antenna circuit of Fig. 4, a, we find the capacitance voltage e_{C_A} and the resistance current i_T satisfying the following equations

$$e_{C_A} = e_A^- - e_A^+, \qquad i_A^- = i_A^+ + i_T \tag{19}$$

where $i_A^+ = i_{C_A} = \tau_{C_A} de_{C_A}/d\tau$ and $i_T = s_T e_A^-$ ($s_T = Z_0/R_T$). With account of relations (15) – (16), the second equation in (19) yields the circuit equation for the antenna node $n = 0$

$$de_{C_A}(\tau)/d\tau = \omega_{C_A}(1 + s_T)U_A(\tau) \tag{20}$$

where $\omega_{C_A} = 1/\tau_{C_A}$, while the current i_A^+ and the voltage e_A^+ are expressed as

$$i_A^+ = i_A^- - i_T = (1 + S_T)U_A(\tau), \tag{21}$$

$$e_A^+ = -e_{C_A}(\tau) - U_A(\tau), \tag{22}$$

respectively.

The parallel connection of N microstrip lines at the node $n = 0$ with account of relations (13) – (14) yields the basic set of equations:

$$i_A^+ = \sum_{n=1}^{N} i_{A_n}^+ = \sum_{n=1}^{N} P_n + \sum_{n=1}^{N} U_n, \tag{23}$$

$$e_A^+ = e_{A_n}^+ = P_n - U_n \quad (n = 1 \ldots N) \tag{24}$$

where $P_n = P_n(\vartheta_n)$ and $U_n = U_n(\vartheta_n - d_n)$.

Eqs. (23) – (24) yield immediately

$$P_n(\vartheta_n) = e_A^+(\tau) + U_n(\vartheta_n - d_n) = -e_{C_A}(\tau) - U_A(\tau) + U_n(\vartheta_n - d_n) \tag{25}$$

and

$$i_A^+ = \sum_{n=1}^{N} P_n + \sum_{n=1}^{N} U_n = 2\sum_{n=1}^{N} U_n(\vartheta_n - d_n) - N e_{C_A}(\tau) - N U_A(\tau). \tag{26}$$

By comparing Eqs. (21) and (26), we find $U_A(\tau)$ expressed via $U_n(\vartheta_n - d_n)$ and $e_{C_A}(\tau)$ explicitly as follows:

$$U_A(\tau)(1 + S_T + N) = 2\sum_{n=1}^{N} U_n(\vartheta_n - d_n) - N e_{C_A}(\tau). \tag{27}$$

At this stage, we choose U_n ($n = 1 \ldots N$) and e_{C_A} as a set of $N + 1$ independent unknown functions and formulate a closed set of $N + 1$ equations in explicit form with respect to these functions.

We re-write each pair of circuit equations (18) as a single equation with respect to i_n and e_n. Presenting e_{C_n} from the second Eq. (18) as

$$e_{C_n} = e_n + e_{B_n} - \tau_{L_n} di_n/d\tau, \tag{28}$$

and substituting this into the first Eq. (18), we obtain N circuit equations with respect to i_n ($n = 1 \dots N$):

$$\tau_{0_n}^2 d^2 i_n / d\tau^2 - \tau_{C_n}(de_n/d\tau + de_{B_n}/d\tau) + i_n - G_n(e_{C_n}) = 0 \tag{29}$$

where $\tau_{0_n}^2 = \tau_{L_n}\tau_{C_n}$ (here, $T_n = 2\pi\tau_{0_n}$ is the intrinsic period of oscillations of LC circuit).

In addition to these N equations for active, resonant, and bias circuits (the equations are of second order, corresponding to the circuit structure), we have also Eq. (20) for the antenna circuit ($n = 0$) which is of the first-order with respect to e_{C_n}. Using the relation (27), we get Eq. (20) closed with respect to functions U_n and e_{C_A}.

By substituting Eqs. (17), Eqs. (9) - (14) and Eqs. (25) into Eqs. (29), we obtain all circuit equations closed and written explicitly in terms of unknown functions U_n and e_{C_A} (functions S_n are expressed via P_n and U_n by using (9), (11), and the first of Eqs. (17), see below).

Thus, the **final set** of $N + 1$ equations in explicit form with respect to $N + 1$ unknown functions U_n and $e_{C_A}(\tau)$ consists of

- *one first-order* Eq. (20) for the antenna circuit ($n = 0$), with substitution of U_A from Eq. (27), and
- N *second-order* equations for active, resonant, and bias circuits ($n = 1 \dots N$), with explicit form of equations being as follows:

$$\begin{aligned} U_n''(\vartheta_n) \;=\; & -P_n''(\vartheta_n - d_n) + \omega_{L_n} e'_{B_n}(\tau) + 2\omega_{L_n}[S_n'(\vartheta_n - 2d_{S_n}) - U_n'(\vartheta_n)] - \\ & \omega_{0_n}^2 [U_n(\vartheta_n) + P_n(\vartheta_n - d_n) - G_n(e_{C_n})] \end{aligned} \tag{30}$$

where $\omega_{L_n} = 1/\tau_{L_n}$, $\omega_{0_n} = 1/\tau_{0_n}$,

$$e_{C_n} = e_{B_n} + 2[S_n(\vartheta_n - 2d_{S_n}) - U_n(\vartheta_n)] - \tau_{L_n}[U_n'(\vartheta_n) + P_n'(\vartheta_n - d_n)], \tag{31}$$

$$P_n(\vartheta_n - d_n) = U_n(\vartheta_n - 2d_n) - e_{C_A}(\tau - d_n) - U_A(\tau - d_n), \tag{32}$$

and

$$S_n(\vartheta_n) = U_n(\vartheta_n) + P_n(\vartheta_n - d_n) - S_n(\vartheta - 2d_{S_n}). \tag{33}$$

An essential feature of Eqs. (30) - (33) is that they are nonlinear differential-difference equations with time delays. They account for both the nonlinearity of devices and the delay of coupling between the devices due to the time needed for the wave propagation along the transmission lines. This property makes the system prone to non-conventional dynamics such as the dynamical chaos and other nonlinear effects that could be useful for various applications.

3.2 Power combining with parallel circuits

In this section, we consider a possibility of power combining in the systems with parallel connection of microstrip circuits described above.

We obtain numerical solutions of the equations derived in section 3.1 by using the integration methods presented in Ref [15], particularly, the Dormand-Prince method of the 8(5+3) order which we extended for the case of time-delay equations specific for our problem.

Being direct time-domain computations, accurate solutions of these nonlinear equations are rather time-consuming. Time sequences of the field evolution were, typically, found for many thousands of intrinsic periods T_n as defined by the system parameters, with the accuracy of solutions specified at the level of $\varepsilon = 10^{-7} \dots 10^{-12}$ [15] sufficient for obtaining stable and reproducible solutions as verified by more accurate test simulations.

Some examples of the field evolution (both the voltage $e_{C_n}(\tau)$ at the diode contacts and the wave form $U_A(\tau)$ radiated from the system into an infinite microstrip line) are shown in Figures below. The oscillations develop in the system as a result of self-excitation in response to the initial switching on the bias voltage $e_{B_N}(\tau)$.

The bias voltage was applied as a sum of bias functions Eq. (3) with various rise-time and voltage parameters chosen so as to set the diode voltage e_{C_n} at the desired value $e_{C_n} = 2.5$ in the unstable NDR domain (Fig. 5) either in a single step or in a few consecutive steps, e.g., with under-shoot or over-shoot, as shown in Fig. 6, a. In most cases, under the condition of slow switching, the switch function does not affect the form of established steady-state oscillations as shown in Fig. 6, b.

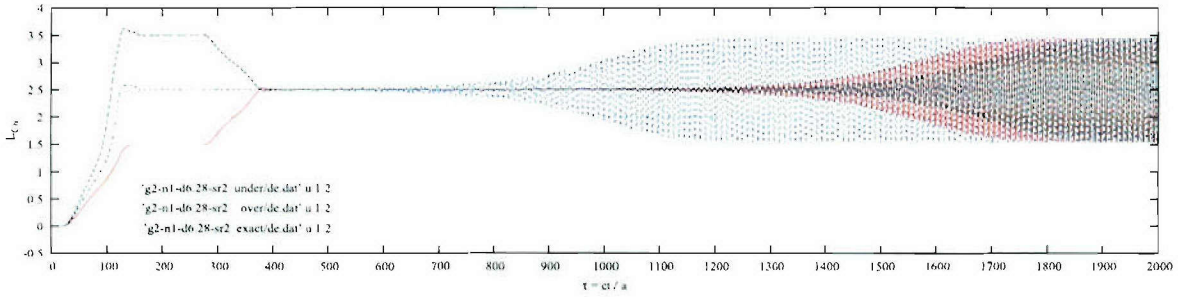

(a)

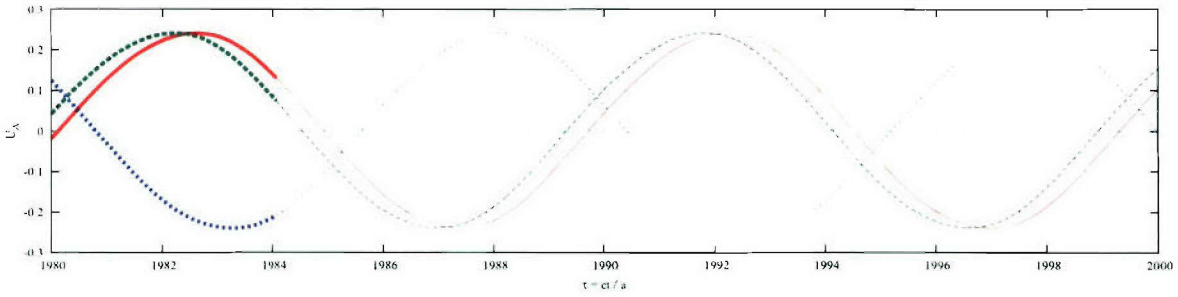

(b)

Figure 6: Self-excitation in the system after switching on the diode voltage $e_G = 2.5$

The space of parameters in this problem is rather large and, therefore, the comprehensive investigation of all cases is not feasible. Instead, one has to focus on the priority issues which are the most useful from both physical and practical points of view. The main questions considered in this work were those concerning the dependences of the generated power P and the basic frequency of oscillations T on (i) the number of active devices N_D in the system, (ii) the lengths d_n and d_{S_n} of microstrip sections, and (iii) the characteristic current G_{0_n} of active devices that defines the typical power output of a single-device system.

Concerning the values of the parameters, we assume the active circuit characteristic times $\tau_{L_n} = \tau_{C_n} = 1$ (the intrinsic period $T_n = 2\pi$), the resonant circuit times being the same as of active circuits, the bias circuit times being small, $\tau_{L_N} = \tau_{C_N} = 0.1$, and the antenna capacitance time being large, $\tau_{C_A} = 10$. In most cases, we assume stubs of zero length, $d_{S_n} = 0$, that significantly simplifies Eqs. (30) – (33), and often assume a zero length of the resonant circuit line $d_{N_{LC}} = 0$ (then, the resonant LC circuit becomes a part of the antenna node). Other parameters different from the above or specific for particular cases are provided in Figure captions.

Using the Gunn diode parameters $I_0 = 8A$ and $V_0 = 30V$ specific for the L-band GaN diodes [13] and assuming the transmission line intrinsic impedance $Z_0 = 50\Omega$, we obtain the dimensionless current parameter $G_{0_n} = Z_0 I_0 / V_0 = 13$ as defined in Eq. (1). With a more conventional type of diodes, e.g., specified by the current $I_0 = 1A$, we may have $G_{0_n} \approx 1$. Therefore, as a typical case, in the following examples we use a moderate value $G_{0_n} = 2$. The diode operation point is specified by the diode voltage $e_G = 2.5$ which is obtained by adjusting

the bias resistance r_B as a function of the number of devices N_D for the fixed bias voltage e_{B_N} chosen as shown for a single-diode system in Fig. 5 (the blue and pink load lines correspond to the bias conductance $s_{B_1} = 2$ and $s_{B_2} = 0.2$, respectively).

The radiation power P is evaluated as the mean power flux of the wave $i_A^-(\tau + x) = U_A(\tau + x)$ radiated from the antenna node $n = 0$ into the open section of transmission line. In relative units, the power of a harmonic wave is evaluated as $P = (1/2)U_A^2$ that is converted to the values in Watts as $P_W = (V_0^2/Z_0)P$. In our examples, assuming $V_0 = 30V$ and $Z_0 = 50\Omega$, the conversion rule is $P_W = 18P$. As an estimate, for the wave of the amplitude $U_A = 0.2$ nearly the same as shown in Fig. 6, b, we find $P = 0.02$ and $P_W = 360mW$. The efficiency of the diode in this case is, however, very low, being estimated as $\eta = P/P_0 = 0.3\%$ where $P_0 = i_G e_G = 6.25$ is the DC power dissipation in the diode.

An example of power combining computed for two nearly identical systems which show quite different dependences of radiation power P on the number of devices is shown in Fig. 7, a. The systems differ only by the value of the bias resistance r_B adjusted as required for the given operation point $e_G = 2.5$ at two different bias voltages specified so that, for a single-diode system, $r_{B_1} = 0.5$ and $r_{B_2} = 5$ (i.e., $s_{B_1} = 2$ and $s_{B_2} = 0.2$) that corresponds to the dashed (green) and solid (red) curves, respectively.

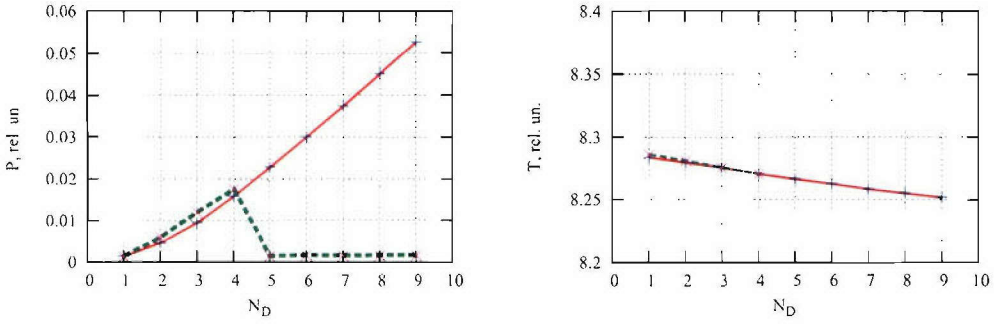

(a) (b)

Figure 7: The power P and the period of oscillations T as functions the number of devices

In the case of a relatively large bias resistance $r_{B_2} = 5$ (red curve in Fig. 7 that corresponds to the pink load line in Fig. 5), the power increases with the number of devices N_D for all tested $N_D = 1 \ldots 9$, growing from $P_W = 23mW$ ($P = 0.0013$) at $N_D = 1$ up to nearly 1 Watt ($P_W = 0.95W$, $P = 0.0526$) at $N_D = 9$.

If, however, the bias resistance is low, $r_{B_2} = 0.5$, the radiation power, after the initial successful growth with the number of devices up to $N_D = 4$, drops drastically to the level only slightly exceeding the power of a single-diode system.

The effect is associated with a variation of basic period of oscillations as shown in Fig. 7, b. With the drastic drop of radiation power in the second case, the basic period jumps from about $T = 8.27$ in relative units (typical for all cases) up to $T \approx 1000$ at $N_D = 5$ (a gradual decrease from this value is observed with increasing N_D that may indicate the possibility of resuming some power growth with a greater number of devices).

It is a known fact that the power combining systems of this kind (including rather successful Kurokawa systems) could be tedious in tuning and exciting. A rigorous time-domain simulation of these systems could significantly improve their understanding and overall design.

3.3 Parametric dependences

None of the systems considered above is the optimal one for the power generation, yet the power grows in some cases is substantial. For the better understanding of the processes involved, we

analyze some parametric dependences in the systems.

First, we consider the dependence of the radiation power on the length $d_{N_{LC}}$ of the resonant LC microstrip section. The radiation power P and the basic period of oscillations T as functions of the length $d_{N_{LC}}$ expressed in the units of intrinsic wavelength λ (the latter is defined formally as $\lambda = T_0 = 2\pi\tau_0$) are shown as an example in Fig. 8.

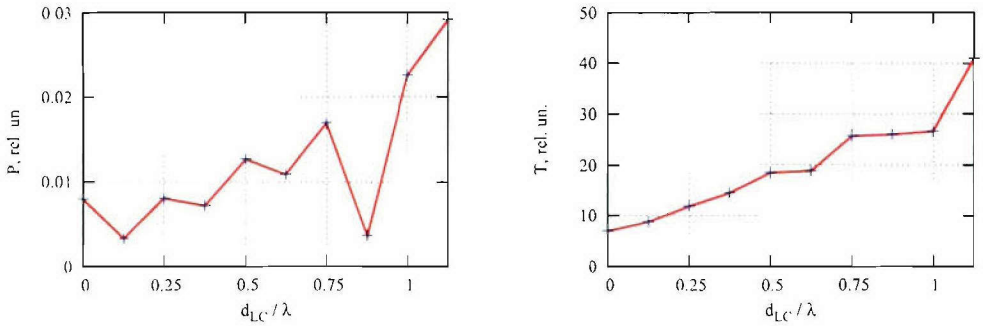

(a) (b)

Figure 8: The power P and the period of oscillations T as functions of $d_{N_{LC}}$

The dependence is rather mild that could justify the choice of the parameter $d_{N_{LC}} = 0$ made in most cases as mentioned above, though we did not make a comprehensive investigation of all the cases. Some examples of the waveforms $U_A(\tau)$ radiated from the system when $d_{N_{LC}} = 0$, $d_{N_{LC}} = \lambda/8$, and $d_{N_{LC}} = \lambda/4$, are shown in Fig. 9.

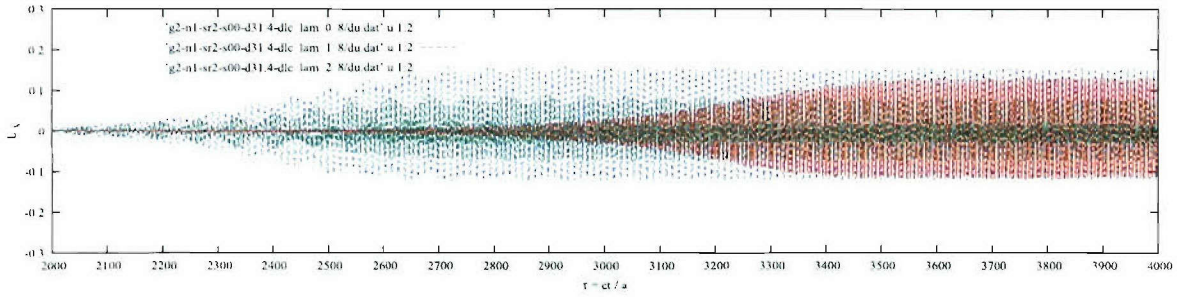

(a)

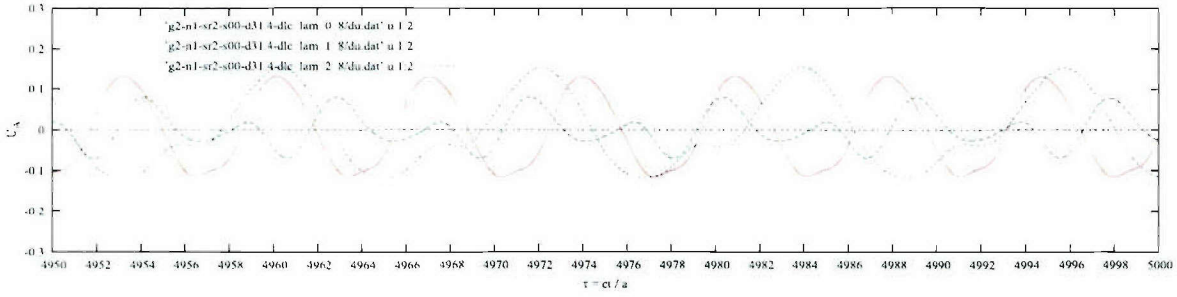

(b)

Figure 9: Waveforms $U_A(\tau)$ radiated from the system when $d_{N_{LC}} = 0,\ \lambda/8,$ and $\lambda/4$

A more informative and important is the dependence of the power P and the basic period of oscillation T on the length of stubs d_{S_n} and of the main sections d_n of microstrip circuits as shown in Figs. 10 – 11. The radiation power P as a function of the stub length d_{S_n} appears to

be about a periodic function with the period close to $\lambda/2$, though this rule is not precise. The oscillation period T varies accordingly, though the variations are not so significant.

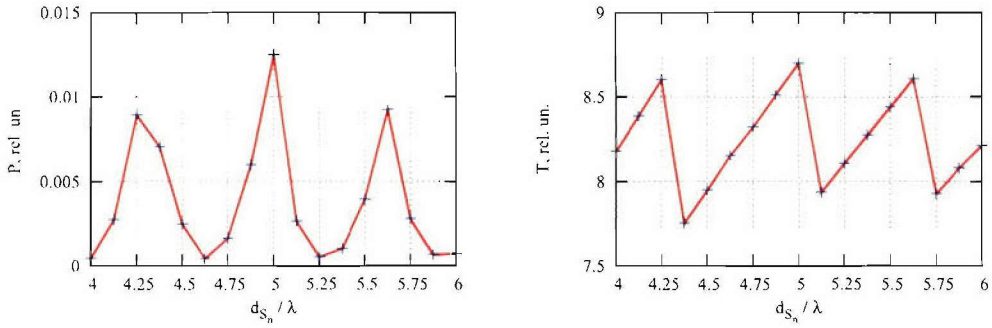

(a) (b)

Figure 10: The power P and the period of oscillations T as functions of the stub length d_{S_n}

The relationship between the locations of power maxima (the values $d_{S_{max}}$ where $P = P_{max}$) and the actual wavelength of radiation ($\lambda_T = T$ in relative units) is not straightforward, being neither precise multiple of $\lambda_T/2$ or $\lambda/2$ (except occasional cases like $d_{S_{max}} = 5$ if comparing $d_{S_{max}}$ with the formal value $\lambda/2$ rather than the actual $\lambda_T/2$).

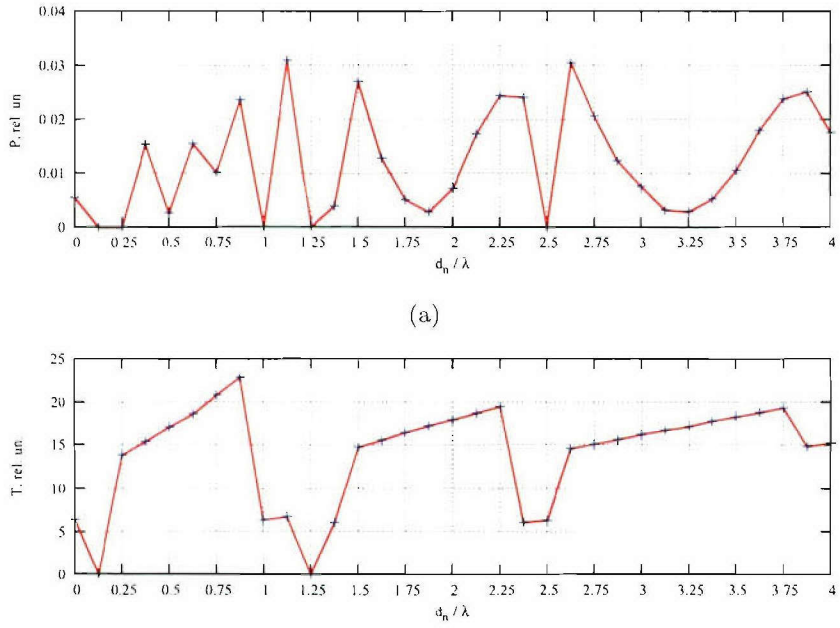

(a)

(b)

Figure 11: The power and the period of oscillations as functions of the microstrip length d_n

Both the period and the location of maxima of radiation power may depend on the nonlinear processes in the system and so on other parameters such as the diode characteristic current G_{0_n}, the number of devices N_D, etc. Therefore, the effect should be investigated specifically (including other effects such as the stability of oscillations etc) for each kind of the system around its possible operation domain.

Fig. 11 shows the radiation power P and the basic period of oscillations T as functions of the microstrip length d_n. This dependence is rather intricate. In the same time, it is rather

stable and robust, being independent of either the way of switching the bias or the accuracy of computations (once it becomes sufficient) as illustrated by the wave profiles shown for various cases in Figs. 12 – 14.

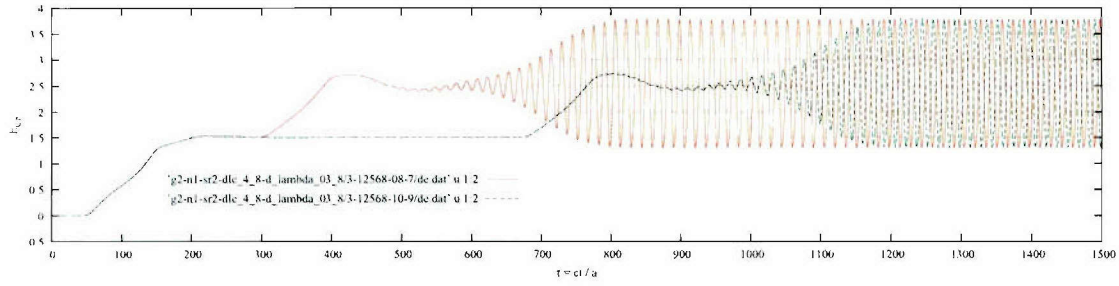

(a)

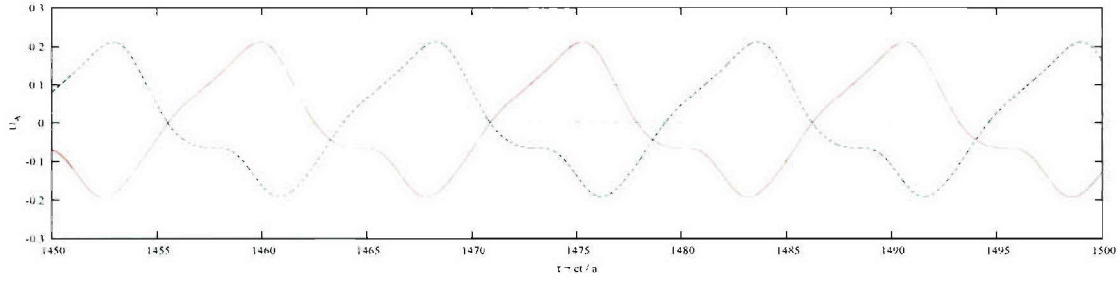

(b)

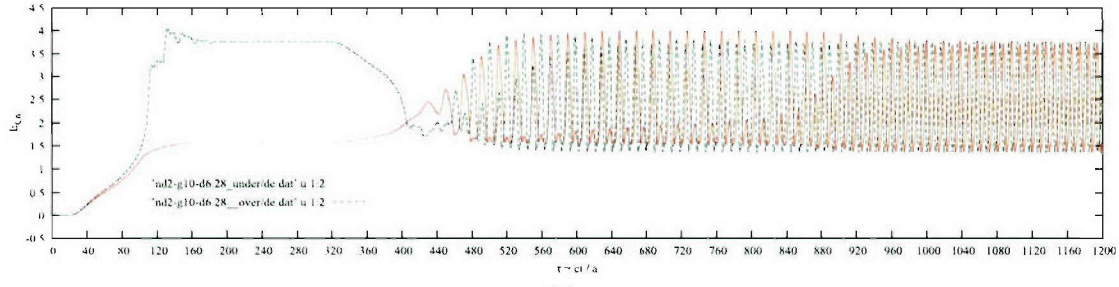

(c)

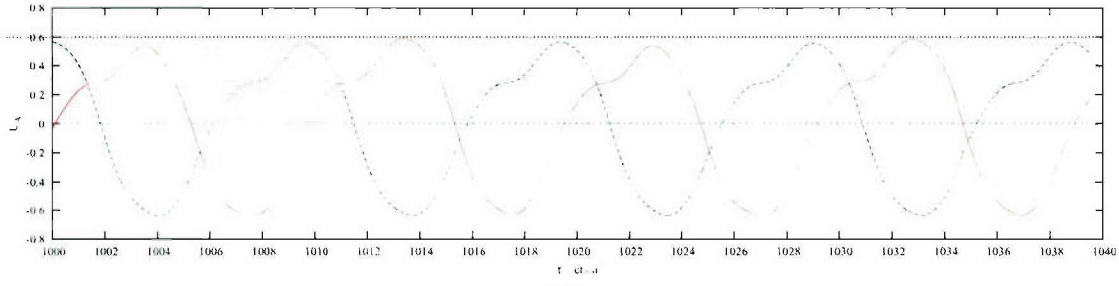

(d)

Figure 12: Robustness of the waveforms with respect to the accuracy and the bias switching

Fig. 12 shows that the waveform excited in the system is insensitive to the accuracy of computation (a and b) when the relative (ε_r) and absolute (ε_a) accuracy of integration are improved from $\varepsilon_r = 10^{-8}$ and $\varepsilon_a = 10^{-7}$ to $\varepsilon_r = 10^{-10}$ and $\varepsilon_a = 10^{-9}$, respectively ($G_0 = 2$, $s_B = 2$, $d_{S_n} = \lambda/2$, $d_n = 3\lambda/8$).

Fig. 12 shows also a similar robustness of the waveform with respect to the bias switching in the system with a strong nonlinearity (c and d) when the Gunn diode characteristic current is $G_0 = 10$ ($d_n = \lambda$).

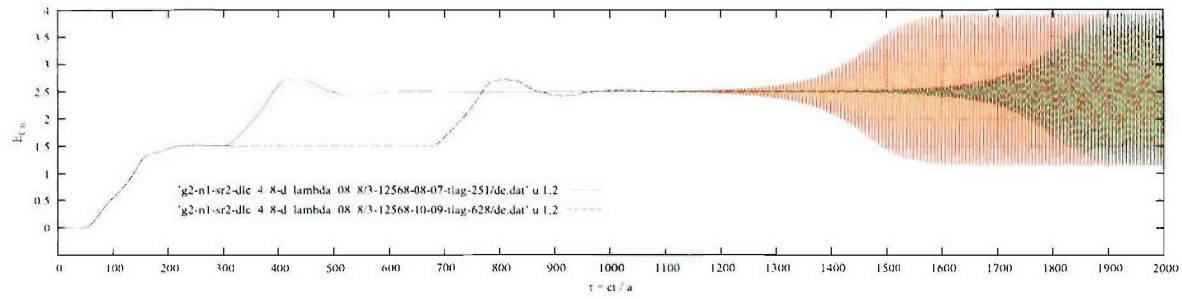

(a)

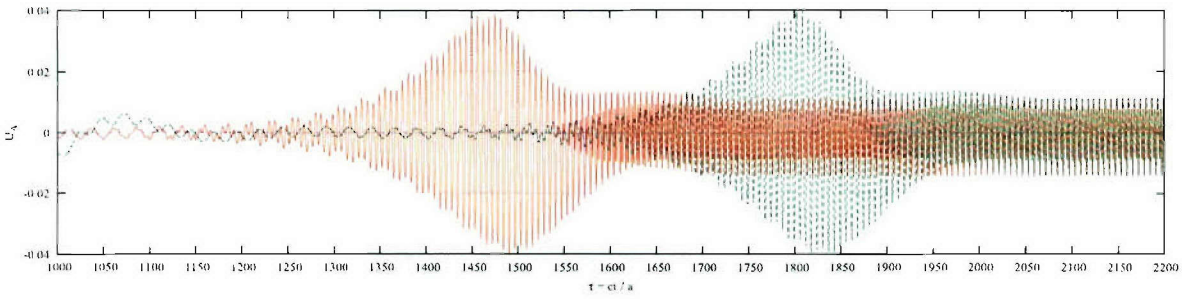

(b)

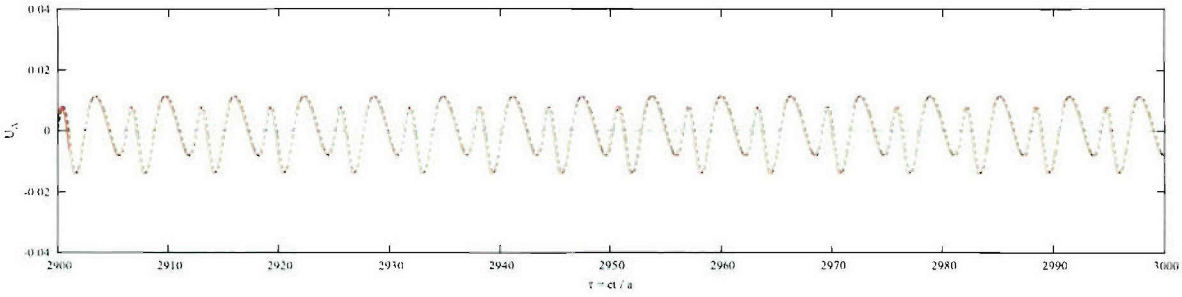

(c)

Figure 13: Waves excited in the system with $d_n = \lambda$ when $G_0 = 2$, $N_D = 1$

Fig. 13 illustrates what happens to the waveform in the process of self-excitation when $d_n = \lambda$ and the radiation power shown in Fig. 11 drops drastically at this value of d_n. The wave profile shows the doubling of the oscillation period T and a significant reduction of the wave amplitude U_A as compared to the initially emerging values. This nonlinear waveform also appears to be insensitive to the accuracy of computation and the bias switch function.

Finally, Fig. 14 compares the wave profiles generated in this system in the case of one and two active circuits when the bias resistance is either $r_B = 5$ or $r_B = 0.5$.

3.4 Summary

- We have developed a mathematical model and computer code for the direct time-domain simulations of the nonlinear electromagnetic self-excitation in the open system of microstrip circuits with active devices (Gunn diodes) in the case of parallel connection of circuits. The results obtained in various cases have shown the feasibility of this approach.

- We carried out self-consistent time-domain simulations of a variety of structures and have shown a possibility of high-frequency power combining in these systems. In the same

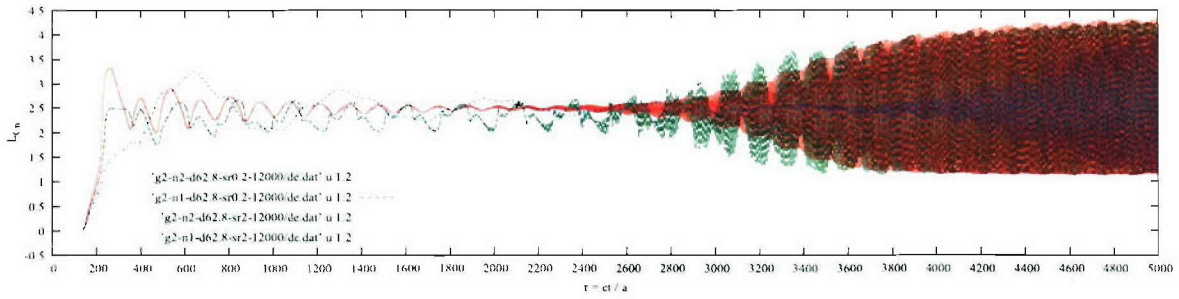

(a)

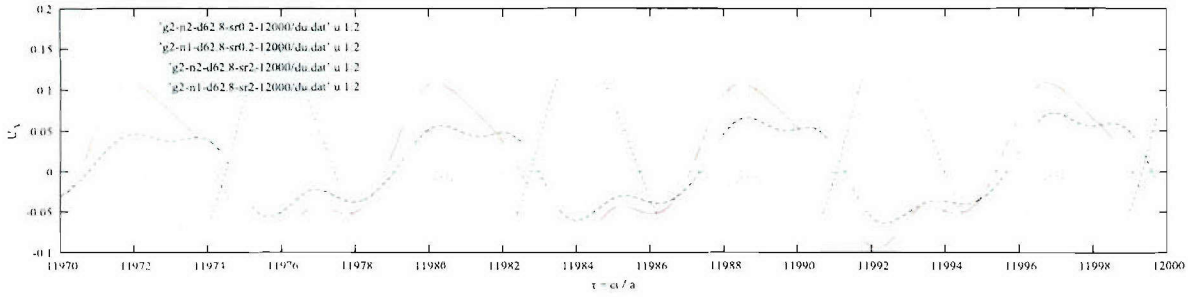

(b)

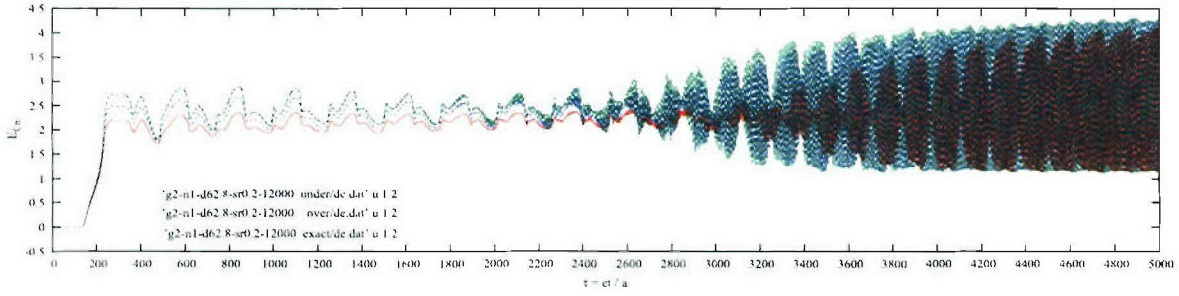

(c)

Figure 14: Waves in the system with one and two diodes when $R_B = 5$ or $R_B = 0.5$

time, we obtained intricate parametric dependences of the output power on the system parameters that illustrates nonlinear character of the processes controlling the efficiency of power combining.

- As an example of non-conventional effects, a drastic drop in the output power with increasing the number of devices has been observed in certain cases as shown in Fig. 7. Because of nonlinear nature of these effects (see, e.g., Fig. 13), various approximate approaches, e.g., those based on the Kurokawa method [1], become inadequate in these cases.

- The microstrip structures mounted on substrates should be rather efficient design solutions in terms of the excess heat dissipation. We, however, simulated only the high-frequency effects and did not consider various engineering features concerning practical implementation of the systems.

- An essential practical problem could be a large value of current in the bias circuit of a system with many devices. This problem may be avoided by using an individual bias circuit for each device, e.g., as shown in Fig. 3, b, though this case has not been simulated so far.

4 Series connection of TL circuits (ladder oscillators)

Since the energy flux of the electromagnetic wave is proportional to the square of the field amplitude, summation of the wave amplitudes from different devices under the condition of phase locking could, in principle, result in a superlinear growth of the radiated power with the number of devices. Despite these considerations, simulations of various one-dimensional systems have shown that, even though such a tendency is observed at a low power level, this does not happen as a general rule.

Since the wave amplitude in the TL circuits of Fig. 1 is, typically, limited by either the current or the voltage, despite the phase locking, the power growth is no more than linear, even though resonant circuits may allow one to increase the amplitude well above the steady-state bias value. Since the same kind of circuitry is inevitably present in the core of any radiating system, a superlinear growth of power with the number of devices is not expected to be likely, except, possibly, the cases of low total power output.

Simulations of a chain of active circuits of Fig. 2, a, mounted in a microstrip line in series as in Fig. 1, b, have shown a possibility of certain superlinear growth of power with increasing the number of devices [10], though, generally, it is accompanied by a significant drop of the oscillation frequency which is, typically, inverse-proportional to the total length of the microstrip structure.

Series connection of active circuits offers, however, other opportunities related to the nonlinear spectrum modifications in these systems as we consider below.

4.1 Formulations for a series connection of circuits

In this section, we consider a series connection of N active circuits of Fig. 2, b, mounted in the microstrip lines as shown in Fig. 1, b [16]. All circuits are supposed to be identical and the initial conditions are assumed to be steady-state voltage and current distributions corresponding to the given diode voltage operation point $e_{Cn}^{(0)}$ chosen within the NDR domain of the current-voltage characteristic Eq (1).

Unlike the circuits simulated in Ref [10] (Fig. 2, a) that partially shunted the high-frequency current components, the circuits in Fig. 2, b, stimulate the propagation of high-frequency waves along the line. In both cases, the character of the effects depends on the TL parameters, particularly, on the lengths of the TL sections between the diodes and on the values of the bias resistance R_n in each section (here we express R_n in relative units instead of r_n).

The equations for the voltages and currents in the circuits and in the TL are obtained in a way similar to the above. With account of the actual type of circuits, the equations for the chain of N diodes are reduced to the set of $2N$ ordinary differential equations of the first order with N time delays $\delta_n = d_n$ of a general form

$$dU_n/d\tau = F_{U_n}(U_n, P_n) \tag{34}$$

$$dP_n/d\tau = F_{P_n}(U_n, P_n) \tag{35}$$

where F_{U_n} and F_{P_n} are the algebraic functions of U_n and P_n with various time delays δ_n and with no delay at the moment of time τ.

Functions U_n and P_n are the profiles of the voltage waves being specified at the circuit locations $x = x_n$ and propagating to the left and to the right from the circuits along the respective sections of the TL.

Functions F_{U_n} and F_{P_n} are specified as follows:

$$F_{U_n}(\theta_n) = F_{U_{n+1}}(\theta_{n+1} - d_{n+1}) - 0.5[F_{C_n}(\theta_n) + F_{L_n}(\theta_n)] \tag{36}$$

$$F_{P_n}(\theta_n) = F_{P_{n-1}}(\theta_{n-1} - d_n) - 0.5[F_{C_n}(\theta_n) - F_{L_n}(\theta_n)] \tag{37}$$

where $n = 1 \ldots N$, $\theta_n = \tau + x_n$,

$$F_{C_n}(\theta_n) = \omega_{C_n}\{U_{n+1}(\theta_{n+1} - d_{n+1}) + P_n(\theta_n) + G_n(e_{C_n})\} + de_{B_n}(\tau)/d\tau \tag{38}$$

$$F_{L_n}(\theta_n) = \omega_{L_n}\{U_n(\theta_n) - P_{n-1}(\theta_{n-1} - d_n) + R_n[U_n(\theta_n) + P_{n-1}(\theta_{n-1} - d_n) - U_{n+1}(\theta_{n+1} - d_{n+1}) - P_n(\theta_n)]\} \quad (39)$$

$$F_{U_{N+1}}(\theta_{N+1} - d_{N+1}) = F_{P_N}(\theta_N - 2d_{N+1}) , \qquad F_{P_0} = 0 \quad (40)$$

and

$$e_{C_n}(\tau) = e_{B_n}(\tau) - U_{n+1}(\theta_{n+1} - d_{n+1}) + P_n(\theta_n) + U_n(\theta_n) - P_{n-1}(\theta_{n-1} - d_n) \quad (41)$$

with the same notations as in Sections 2 and 3.

The steady-state initial conditions at the voltage operation point $e_{C_n}^{(0)}$ correspond to the initial bias $e_{B_n} = e_{C_n}^{(0)}$ $(n = 2 \dots N)$ and $e_{B_1} = e_{C_1}^{(0)} + R_1 G_1(e_{C_1}^{(0)})$ that results in the initial values of U_n and P_n defined as follows:

$$P_0 = 0.5 R_1 G_1(e_{C_1}^{(0)}) , \quad U_1 = -P_0 \quad (n = 1), \quad (42)$$

$$P_{n-1} = -0.5 G_n(e_{C_n}^{(0)}) , \quad U_n = P_{n-1} \quad (n = 2 \dots N). \quad (43)$$

The excitation appears as a result of a small bias fluctuation that reduces to zero later on.

4.2 Analytical Treatment

In the case of a single diode $N = 1$ with a stub of length d, we could obtain some analytical results and compare them with numerical simulations. In this case, we can apply the concept of zero impedance conditions [1], $Z = 0$, to find the frequencies of emerging self-oscillations and to verify this concept against exact numerical solutions. The conditions of $\mathrm{Re}(Z)$ and $\mathrm{Im}(Z)$ constitute a pair of equations that can be written in the form

$$\{\omega_0^2(Z_G + R) - \omega(\omega_L Z_d + \omega) Z_G\} Z_r = \omega Z_d(\omega_L Z_G R + \omega_C) - \omega_0^2 Z_G R \quad (44)$$

$$\{\omega_0^2 Z_d + \omega(\omega_L Z_G R + \omega_C)\} Z_r = \omega(\omega Z_d - \omega_C) Z_G - \omega_0^2 Z_d R \quad (45)$$

where Z_r is the effective impedance of the radiating TL section (the antenna radiation resistance), $\omega_0^2 = \omega_L \omega_C$, $Z_S = iZ_d(\omega) = i\tan(\omega d)$ is the impedance of the stub of length d at the circular frequency ω and $Z_G = 1/(dG/de_C)$ is the diode impedance at the voltage operation point e_{C_0}, all being defined in relative units.

In an open system, the effective impedance Z_r (a real number that represents an ideal sink of energy at the infinity) is unknown in advance, unlike the load impedance in a closed non-radiating circuit. Eqs. (44) and (45) define the same value of the impedance Z_r, thus providing the equation for the frequency ω that can be written in the form

$$Z_d^2(\omega)\omega\omega_L(\omega^2 Z_G^2 + \omega_C^2) + Z_d(\omega)\{\omega^4 Z_G^2 + \omega^2[(\omega_L Z_G - \omega_C)^2 + \omega_L^2 Z_G^2(R^2 - 1)] + \omega_0^4 R^2\} + \omega\omega_C Z_G^2(\omega_0^2 - \omega_L^2 R^2 - \omega^2) = 0. \quad (46)$$

Roots of Eq. (46) with proper treatment of singularities and spurious solutions to satisfy Eqs. (44) and (45) define the spectrum of oscillations. If there is no stub ($d = 0$), Eq. (46) has a single frequency solution independent of Z_G,

$$\omega = \omega_0\sqrt{1 - R^2\omega_L/\omega_C} \quad (47)$$

with $Z_r = -Z_G\omega_C/(\omega_C + Z_G R\omega_L)$ (here $Z_G < 0$ and $Z_r > 0$ if e_{C_0} is in the NDR domain). If, however, a stub is connected ($d \neq 0$), Eq. (46) defines a multi-frequency spectrum that essentially depends on the diode impedance Z_G.

Eqs. (34) – (41) yield the dispersion relation for small oscillations $u, p \approx \exp(i\omega\tau)$ around the steady-state condition of Eqs. (42). If $d = 0$, the relation is

$$\omega^2 - i\omega[\omega_L R + \omega_C(Y_G + 1)] - \omega_0^2[1 + (Y_G + 1)R] = 0 \quad (48)$$

where $Y_G = 1/Z_G$ is the diode admittance.

Eq. (48) shows that small initial fluctuations grow up if $(Y_G + 1) < -R\omega_L/\omega_C$, though they can turn into oscillations if only $|(Y_G + 1)\omega_C - R\omega_L| < -2\omega_0$ (otherwise, switching from the unstable initial condition, $Z_G < 0$, to one or another stable condition, $Z_G > 0$, occurs in the system as predicted by Eq. (48) and, indeed, observed in simulations).

Notice that, even though Eq. (48) seems to fully determine the frequency ω, in reality, it is the balance of gain versus losses expressed by Eqs. (44) and (45) that controls the dominant frequencies in the spectrum of the established self-oscillations in a small-signal mode considered above.

4.3 Spectrum of oscillations

Conditions for self-excitation of the system and the spectrum of small oscillations could be found by considering zeros and singularities, as functions of the frequency, of impedance or admittance of the TL circuits defined with respect to different ports [1]. Time-domain simulations based on Eqs. (34) - (41) confirm these considerations in basic features, though specific details are more complicated [16].

First, we consider the case of one active circuit $N = 1$. In this case, we study the circuits with the stubs of zero length ($d = 0$, compact open circuits) and of nonzero lengths (extended circuits of size d). We adjust the values of the diode current parameter G_0 (proportional to the diode admittance) to generate the oscillations of either small or large amplitude. We also vary other parameters for testing the validity and limitations of the analytical solutions found above.

In a circuit with no stub ($d = 0$), when G_0 is just sufficient for self-excitation estimated by Eq. (48), we obtain small oscillations ($u \approx 0.1$) at a single frequency predicted by Eq. (47) as shown in Fig. 15, a ($R = 0$, 5, 9 at $\omega_L = 0.1$, $\omega_C = 10$ for the solid, dashed and dotted lines, when $\omega = 1$, 0.866, and 0.436, respectively).

With increasing the diode admittance in the domain of oscillatory solutions, the basic frequency decreases approaching zero (when the oscillations are replaced by switching) and higher harmonics appear. The spectrum remains, however, rather simple, with just a few harmonics of relatively small amplitude being present, Fig. 15, b.

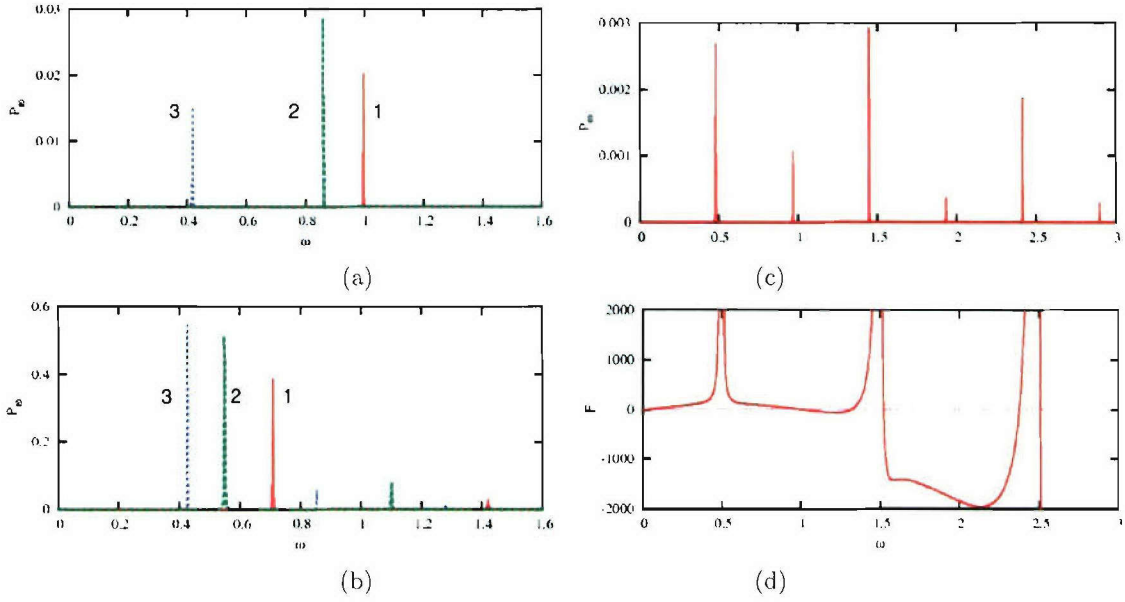

Figure 15: Spectrum of radiation from a single circuit when (a) $d = 0$ at small $G_0 = 11...12$, (b) $d = 0$ at large $G_0 = 14...16$ ($R = 0...5$), (c) $d = \lambda_0/2$ at small G_0 ($G_0 = 2$) and (d) the left-hand part of Eq. (46) in case (c)

In a circuit with a stub, we observe small oscillations at multiple frequencies as expected from Eq. (46). Fig. 15, c, shows the spectrum of small-signal radiation from the circuit with the stub of length $d_0 = \lambda_0/2$ resonant with the frequency $\omega_0 = 1$ ($Z_d(\omega_0) = 0$, $d_0 = \pi$) when $\omega_L = 0.1$, $\omega_C = 10$, $G_0 = 2$, and $R = 0$. The spectrum is consistent with the roots and singularities of the left-hand part of Eq. (46) as Fig. 15, d, shows. The excitation of circuits with a stub appears possible at very small G_0, e.g., even with $G_0 < 0.2$ in this example as compared to $G_0 > 11.2$ ($R = 0$) in a similar circuit with no stub in Fig. 15, a (if $Z_0 = 50\Omega$, GaN diode parameters correspond to $G_0 = 13$).

In a nonlinear mode, the spectrum of radiation from a circuit with a stub has little in common with the spectrum predicted by Eq. (46) at the relevant value of G_0 (both spectra vary significantly with G_0). With increasing G_0, the oscillations remain multi-frequency with rather narrow spectral lines, though the basic frequency decreases like in the case of a circuit with no stub.

More interesting effects are observed in the chain of N circuits. With increasing N, we observe broadening of spectral lines alone with increasing the number of lines as shown in Fig. 16, a. The effect appears even in a regular chain of identical circuits with TL sections of the same length d (a stub of the last circuit is of length $d/2$) if $R = 0$ (solid curve) while the lines remain narrow if there is a significant resistance in each circuit (e.g., $R = 5$, dotted lines).

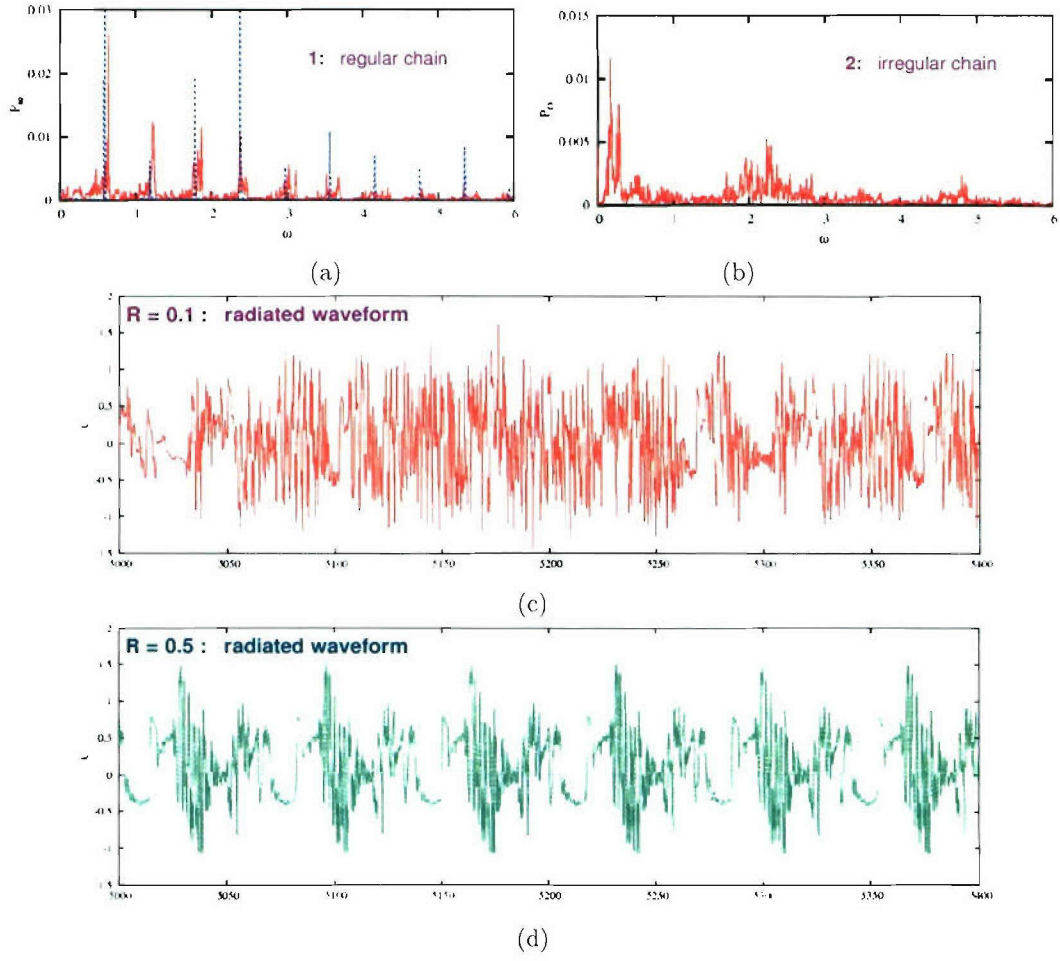

Figure 16: Spectrum of radiation from a chain of circuits similar to those in Fig. 15, c, when (a) $d_n = d = 5$ and (b) $d_1 = 6.91$, $d_2 = 3.77$, $d_3 = 8.17$, $d_4 = 3.14$ (in both cases, $G_0 = 13$) and the radiation waveform in the latter case if (c) $R = 0.1$ (spectrum b) and (d) $R = 0.5$ (spectrum is very similar to b)

If the chain is irregular, e.g., with different lengths of TL sections, the broadening of spectral lines is more significant, the spectrum could be quasi-continuous, Fig. 16, b, and the radiated wave rather chaotic, Fig. 16, c). This effect could signify the transition to the dynamical chaos, though it requires more careful examination. The waveform looks rather chaotic during the whole long time of computation if R is small (Fig. 16, c, was computed with $R = 0$ up to $\tau = 8000$) but switches to a regular pattern after an extended period of time τ_s if R is not too small ($\tau_s = 1400$ if $R = 0.5$, Fig. 16, d). Both spectra, however, are remarkably similar, having a distinctive quasi-continuous component.

4.4 Non-conventional dynamics: chaos and pulses

Recent simulations of structures with time-delay coupling of active devices indicated a possibility of non-conventional dynamics in these systems such as the dynamical chaos [17] and the excitation of trains of high-frequency pulses [18]. A series connection of active circuits with significant time-delay coupling between circuits is one of typical cases that could result in the dynamical chaos of electromagnetic field, though the effect was simulated using a simplistic model of an instant response of active circuits to the external field assuming $\tau_L = \tau_C = 0$.

The results of our research show that, in the case of non-instant circuit response represented by reactive components in Figs. 2 – 4 ($\tau_L \neq 0$, $\tau_C \neq 0$), the dynamical chaos remains a possibility under certain conditions. In order to detect the presence of the dynamical chaos, we perform some basic tests such as the construction of the Poincare sections (Fig. 17), computation of the correlation functions (Fig. 18), and the study of divergence of adjacent trajectories [16].

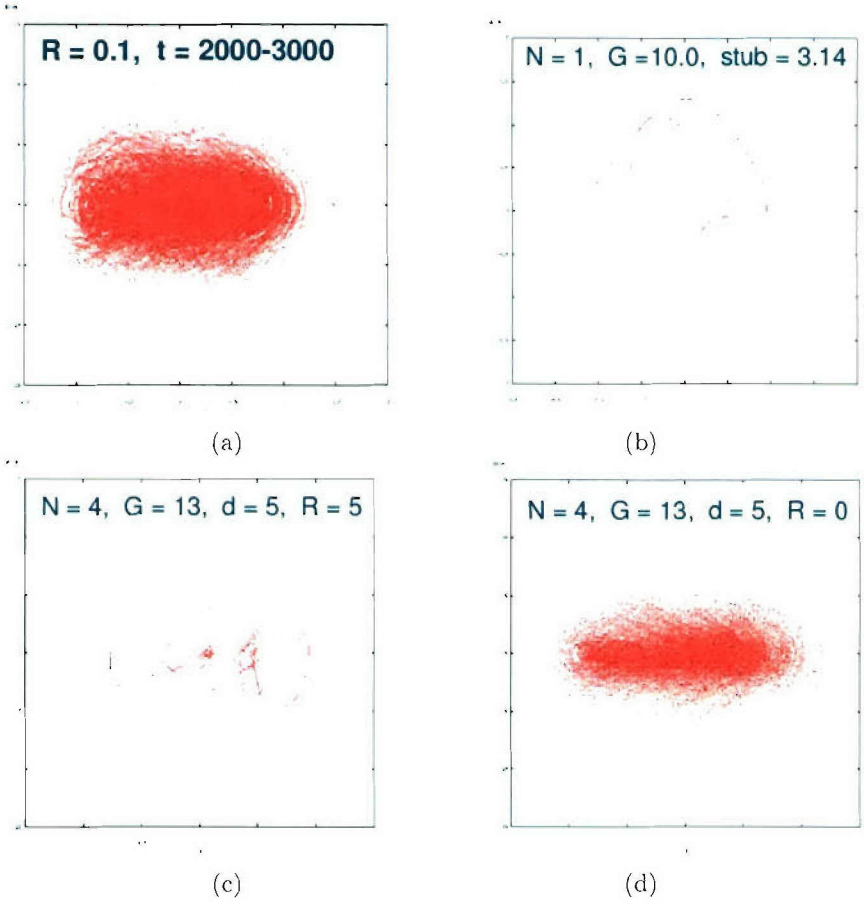

Figure 17: Poincare sections showing the complicated dynamics of the electromagnetic field in microstrip structures with a series connection of active circuits

As an example, Fig. 17, a, shows the Poincare section computed with the waveform radiated from the structure, Fig. 16, c, whose spectrum is shown in Fig. 16, b (irregular chain of $N = 4$ active circuits with $R = 0.1$, $G_0 = 13$). This is a typical phase portrait of the system with the dynamical chaos.

For the comparison, Fig. 17, b – d, presents some other cases where one can observe (b) the period doubling as a canonical route to chaos (one circuit with a stub, $N = 1$, $G_0 = 10$, $d = 3.14$, $R = 0$), (c) complicated multi-frequency generation (regular chain of $N = 4$ circuits with $G_0 = 13$, $d = 5$, $R = 5$), and (d) chaotic Poincare section of the system whose spectrum is shown in Fig. 16, a (regular chain of $N = 4$ circuits with $G_0 = 13$, $d = 5$, $R = 0$) which does not look as purely chaotic but rather as a combination of multi-frequency generation and some chaotic component at a low level.

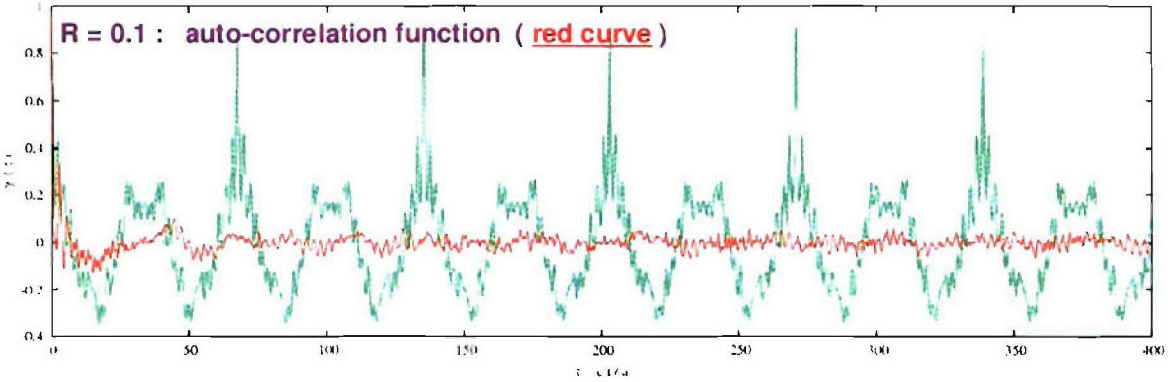

Figure 18: Auto-correlation functions of the radiation field of irregular chain of $N = 4$ active circuits ($G_0 = 13$) when $R = 0.1$ (red solid curve) and $R = 0.5$ (green dashed curve)

Fig. 18 shows the auto-correlation function of the waveform presented in Fig. 16, c, which reveals a low level of correlations in the radiation signal (red solid curve). For the comparison, the green dashed curve presents the auto-correlation function of the waveform shown in Fig. 16, d. In this case, a regular periodic, yet complicated waveform develops, which is of such a kind that both the frequency spectrum (which is similar to Fig. 16, b) and the Poincare section look rather chaotic, yet the auto-correlation function shows a very definite periodicity in the revivals of auto-correlations.

Another dynamical effect of potential practical interest is the generation of trains of high-frequency pulses in the systems where an active circuit is separated from a compact (e.g., lumped) high-frequency resonator by a relatively long section of transmission line providing a time-delayed feedback, while the pulses are radiated from the resonator into an infinite section of the TL, thus, simulating the electromagnetic wave radiation into the outer space, Fig. 19.

These trains of pulses are similar to those simulated earlier in a one-dimensional cavity with a thin dielectric mirror [18], [19] where the mirror served as a compact resonator. Compared to those simulations, this TL model with Gunn diodes is more rigorous since the model accounts for a non-instant response of active circuits to the external field ($\tau_L \neq 0$, $\tau_C \neq 0$). On the other hand, it uses a generic LC-circuit as a compact resonator (which is equivalent to the dielectric mirror) between an active TL section and an infinite section of transmission line, thus, showing a generic nature of self-emergence of trains of pulses in the systems with time delay.

4.5 Summary and further research

- Simulations of a chain of TL circuits of Fig. 2, a, have shown a possibility of power combining [10] which is accompanied by significant decrease of the oscillation frequency, with more complicated effects emerging in the lines with long inter-device TL sections.

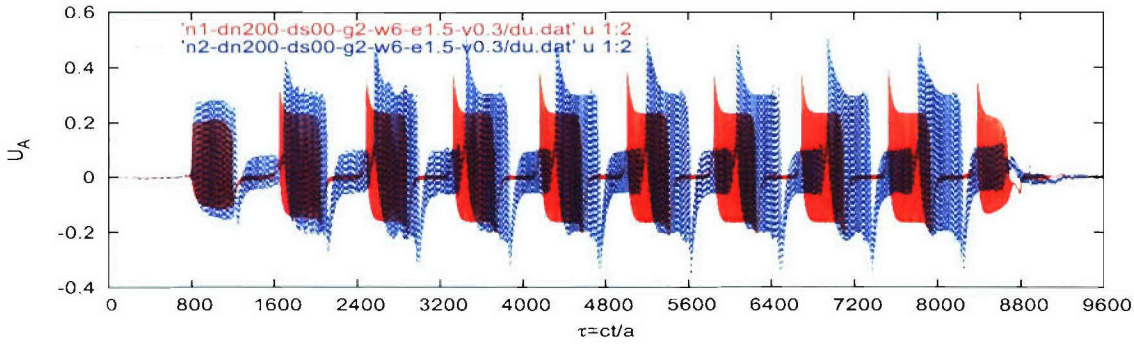

(a)

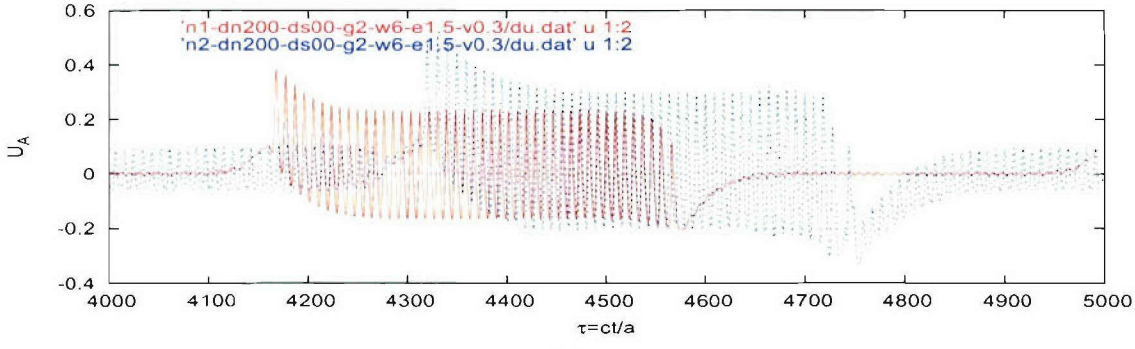

(b)

Figure 19: Trains of high-frequency pulses generated in the microstrip line of Fig. 1, a, with $N = 1$ (red solid curve) and $N = 2$ (blue dotted curve) active circuits as in Fig. 3, a, and a resonant antenna circuit $n = 0$ as in Fig. 4, b ($d_n = 200$, $d_{S_n} = 0$, $G_0 = 2$)

Final equations in [10] were, however, not of the most optimal form. Therefore, improved simulations are needed to clarify various issues related to the nonlinear effects in the long TL structures.

- Nonlinear time-delay coupling in the chains of TL circuits of Fig. 2, b, simulated in this work could produce broadband dynamical chaos or self-sustained generation of trains of high-frequency pulses. The effects of this kind could be of potential interest for novel radar technologies as presented in Ref [11]. These effects, however, are rather complicated and require more comprehensive investigations.

- For the efficient power combining at high frequencies, other kinds of circuits (e.g., as those shown in Fig. 3, b) with parallel connection of TL sections and separate bias of each device (with account of extended length of the bias lines which should affect the device operation, and also with or without the common power supply feeding these separate bias lines) have to be simulated. Therefore, further research is needed to explore these and other possibilities of high-frequency power combining, including also a possibility of superlinear growth of power.

- A major drawback of all the models considered is the neglect of intrinsic dynamics of active devices. This is caused by significant complexity of the internal processes responsible for the device operation (e.g., the dynamics of strong-field domains in Gunn diodes, etc). A more realistic modeling of TL circuits with active devices requires an efficient (and so, reasonably simplified) modeling of internal processes in the devices and their self-consistent

account in the simulations of the whole TL systems.

- Other kinds of active THz devices such as resonant tunneling diodes, especially, novel interband-RTD with enhanced frequency and power output [20], or arrays of quantum dots with suppressed electron scattering [21], [22], have to be considered because of much higher operation frequencies of these devices. For this, with account of complicated internal dynamics of the devices [23], [24], reasonably simplified theoretical models of relevant structures have also to be developed.

5 Conclusions

We carry out time-domain simulations of nonlinear self-excitation of active systems with Gunn diodes connected by extended sections of microstrip transmission lines (TL) and radiating the electromagnetic waves into an infinite open line. Various models of distributed circuits of this kind have been studied, with parallel, series, and mixed coupling of active elements in the TL network.

One-dimensional transmission line models, in distinction from computationally involved 3D structures, allow us to develop more rigorous formulations and obtain accurate self-consistent solutions, with the conclusions that could be generalized to other cases.

Practical issues of interest are the possibility of nonlinear power combining of active devices in distributed circuits of the open kind and the emergence of non-conventional dynamics in such systems due to strong nonlinear time-delay coupling between many devices. For the efficient modeling of these systems, we consider simplified one-dimensional TL models representing the wave guiding properties of microstrip structures, though neglecting small dispersion and radiation losses of real systems.

Power combining is shown to occur in both parallel and series connections of active devices in these distributed systems, though, typically, the power growth is no more than linear in the number of devices N_D despite an efficient phase locking. Power growth shows a tendency to saturate at large N_D and, in the case of series connection of devices in the ladder circuits, is associated with decreasing the basic frequency of oscillations.

Complex dynamics of the electromagnetic field radiated into an open end of the TL are observed in special cases in the simulations of series connections of active circuits. A chain of devices mounted in an open line with irregular spacings between the devices could generate chaotic electromagnetic signals for ultra-wideband applications such as noise radars and similar systems. The chaos in many cases could be accompanied by multi-frequency generation.

In special cases, when active devices are separated from compact resonant circuits by extended sections of the transmission lines, trains of high-frequency pulses are radiated from the system in a self-sustained manner, with the pulsing period being defined by the length of the microstrip section providing the time-delayed feedback.

Acknowledgement

Effort was sponsored by the Air Force Office of Scientific Research, Air Force Material Command, USAF, under grant number FA8655-04-1-3027. The U.S. Government is authorized to reproduce and distribute reprints for Governmental purpose notwithstanding any copyright notation thereon.

References

[1] K. Kurokawa, "The Single-Cavity Multiple-Device Oscillator," *IEEE Trans. Microwave Theory Techn.*, Vol. MTT-19, pp. 793 – 801, 1971.

[2] K. J. Russell, "Microwave Power Combining Technique," *IEEE Trans. Microwave Theory Techn.*, Vol. MTT-27, pp. 472 – 478, 1979.

[3] J. W. Mink, "Quasi-Optical Power Combining of Solid-State Millimeter-Wave Sources," *IEEE Trans. Microwave Theory Techn.*, Vol. MTT-34, pp. 273 – 279, 1986.

[4] M. P. DeLisio and R. A. York, "Quasi-Optical and Spatial Power Combining," *IEEE Trans. Microwave Theory Techn.*, Vol. MTT-50, pp. 929 – 936, 2002.

[5] P. H. Siegel, "Terahertz Technology," *IEEE Trans. Microwave Theory Techn.*, Vol. MTT-50, pp. 910 – 928, 2002.

[6] S. Y. Liao. *Microwave Circuit Analysis and Amplifier Design*, Prentice-Hall, New Jersey, 1987.

[7] C. A. Lee and G. C. Dalman, *Microwave Devices, Circuits and their Interaction*, John Willey and Sons, New York, 1994.

[8] A. Taflove and S. C. Hagness, *Computational Electrodynamics: the Finite-Difference Time-Domain Method*, Artech House, New York, 2000.

[9] V. B. Erturk, R. G. Rojas, and P. Roblin, "Hybrid Analysis/Design Method for Active Integrated Antennas," *IEE Proc. - Microw. Antennas Propag.*, Vol. 146, pp. 131 – 137, 1999.

[10] V. Yurchenko and L. Yurchenko, "Time-Domain Simulation of Power Combining in a Chain of THz Gunn Diodes in a Transmission Line," *Int. J. Infrared and Millimeter Waves*, Vol. 25(1), pp. 43 – 54, 2004.

[11] K. A. Lukin, "Noise Radar Technology for Short Range Applications," in *The 5th Int. Conf. on Radar Systems*, Brest, France, May 1999.

[12] M. Shur, *GaAs Devices and Circuits*, Plenum Press, London, 1987.

[13] E. Alekseev and D. Pavlidis, "GaN Gunn Diodes for THz Signal Generation," in *IEEE MTT-S Int. Microwave Symposium Digest*, pp. 1905 – 1908, 2000.

[14] K. A. Lukin et al., "Method of Difference Equation in the Resonator Problem with a Nonlinear Reflector," *Soviet Physics - Doklady*, Vol. 34, pp. 977 – 979, 1989.

[15] E. Hairer E. and G. Wanner, *Solving Ordinary Differential Equations II: Stiff and Differential-Algebraic Problems*, Springer-Verlag, Berlin, 1991.

[16] V. B. Yurchenko and L. V. Yurchenko, "Self-Excitation of a Chain of Gunn Diodes Connected by Transmission Lines," in *URSI-Turkey'2004 Symposium*, Bilkent University, Ankara, Turkey, Sept. 8-10, 2004, pp. 460 – 462.

[17] L. V. Yurchenko and V. B. Yurchenko, "Analysis of the Dynamical Chaos in a Cavity with an Array of Active Devices," in *The 12th Int. Conf. on Microwaves and Radar (MIKON'98)*, Warsaw, Poland, 1998, Vol. 3, pp. 20 – 22.

[18] V. B. Yurchenko and L. V. Yurchenko, "Self-Generation of Ultra-Short Pulses in a Cavity with a Dielectric Mirror Excited by an Array of Active THz Devices," in *Proc. 8th Int. Conf. on Terahertz Electronics*, Darmstadt, Germany, Sept. 28-25, 2000, pp. 49 – 52.

[19] L. V. Yurchenko and V. B. Yurchenko, "Ultra-short Pulses Generation in a Cavity with an Active Layer and a Dielectric Mirror," *Applied Radio Electronics*, No. 2, 2005.

[20] D. Woolard, W. Zhang, and B. Gelmont, "A Novel Interband-Resonant Tunneling Diode (I-RTD) Based High-Frequency Oscillator," *Sol.-St. Electron.*, Vol. 49, pp. 257 – 266, 2005.

[21] I. A. Dmitriev and R. A. Suris, "Damping of Bloch Oscillations in Quantum Dot Superlattices: A General Approach," *Semiconductors*, Vol. 36, No. 12, pp. 1364 – 1374, 2002.

[22] I. A. Dmitriev and R. A. Suris, "Damping of Bloch Oscillations in One-, Two-, and Three-Dimensional Quantum Dot Superlattices," *Semiconductors*, Vol. 36, No. 12, pp. 1375 – 1384, 2002.

[23] O. Pinaud, "Transient Simulations of a Resonant Tunneling Diode," *J. Appl. Phys.*, Vol. 92, pp. 1987 – 1994, 2002

[24] V. F. Elesin, I. Yu. Kateev, and A. I. Podlivaev, "A Nonlinear Theory of Coherent Oscillations in a Resonance-Tunnel Diode in a Wide Frequency Range," *Semiconductors*, Vol. 34, No. 11, pp. 1321 – 1326, 2000.